Journal of Pharmaceutical Innovation (2026) 21:620
https://doi.org/10.1007/s12247-026-10815-4

RESEARCH

A Promising Insight into the Treatment of Triple-negative Breast Cancer with Curcumin loaded 1,4-Bis(3-aminopropyl) Piperazine Functionalized-graphene Quantum Dots: Synthesis, Cytotoxicity and In Silico Analyses

Dilara Alver[1] · Pinar Sen[1] · Serap Yalçin Azarkan[2] · Dolunay Şakar[3] · Muhsin Konuk[4]

Received: 22 December 2025 / Accepted: 3 June 2026
© The Author(s) 2026

Abstract
Triple-negative breast cancer (TNBC) is a clinical problem because of its poor prognosis, aggressive behavior, and lack of targeted therapies. Thus, there is an urgent need to find effective evolving therapies that are specific and have few adverse consequences for triple-negative breast cancer. This study aimed to demonstrate that curcumin (Cur), which is the active ingredient of turmeric and is known to exhibit various biological properties, was conjugated to graphene quantum dots (GQDs), resulting in curcumin-loaded GQDs (Cur-GQDs) to overcome its poor solubility properties that limit its pharmacological potential, leading to high anticancer activity compared to curcumin alone. This conjugation (Cur-GQDs) was performed through π-π stacking, forming negatively charged and monodisperse supramolecular hybrids in aqueous solution. Molecular docking analyses revealed that Cur-GQDs structures exhibit high binding affinity against various cancer-related target proteins, and this binding shows a strong correlation with the observed anticancer activity. Additionally, in vitro cytotoxicity and cell migration tests performed on the MDA-MB-231 cell line, which is used as a TNBC cell model, showed that Cur-GQDs produced significantly higher anticancer effects compared to free curcumin application. The findings suggest that combining curcumin with nanotechnological carrier systems like GQDs could be a promising strategy to increase therapeutic efficacy and reduce side effects in the treatment of TNBC. This study demonstrates that the combination of natural compounds with nanostructures can be considered an innovative approach in difficult-to-treat cancer subtypes such as TNBC.

Keywords Curcumin · Graphene quantum dot · Breast cancer · Triple breast cancer · MDA-MB231

Introduction

Cancer, one of the most feared diseases of the 20th century, continues to spread frequently in the 21st century. One in four people is at risk of developing cancer during their lifetime [1]. Cancer can occur because of the abnormal proliferation of any of the cells in our body. As a result, there are over a hundred types of cancer, and their response to treatment and behavior can vary significantly. Cancer cells proliferate continuously and unregulated. They do not respond appropriately to the signals that control cell behavior and grow and divide uncontrollably, invading normal tissues and organs and ultimately spreading throughout the body. Although there are many types of cancer, a few are the most common [2]. One of the biggest health problems worldwide is breast cancer, which is the most common malignant

✉ Pinar Sen
pinar.sen@uskudar.edu.tr

1 Department of Chemical Engineering, Üsküdar University, Üsküdar, Istanbul 34662, Türkiye

2 Depatment of Medical Pharmacology, Kırşehir Ahi Evran University, 40100 Kırşehir, Türkiye

3 Department of Chemistry, Yildiz Technical University, Esenler, Istanbul 34220, Türkiye

4 Department of Molecular Biology and Genetics, Üsküdar University, Üsküdar, Istanbul 34662, Türkiye

Published online: 19 June 2026

tumor [3]. TNBC is a breast cancer subtype that is progesterone receptor negative, estrogen receptor negative, and human epidermal growth factor receptor 2 (HER2) negative according to immunohistochemistry tests and is characterized by heterogeneity, aggressive nature, and significant differences in forms of metastasis and absence of targeted therapy [4].

Radiotherapy, surgery, and chemotherapy are the most widely used traditional treatment methods for cancer [5]. Finding effective therapy to treat patients with TNBC is the biggest challenge for breast cancer. Traditional targeted methods cannot be applied to TNBC patients [6].

Curcuma Longa, also known as turmeric, is a plant of Indian origin belonging to the Zingiberaceae, also known as the ginger family, and cultivated in various parts of the world. Curcumin, as an active ingredient of turmeric, has broad anti-inflammatory and anti-cancer properties. Curcumin's ability to influence gene transcription and trigger apoptosis in preclinical models supports its probable use in chemotherapy and cancer chemoprevention [7].

Constitutive activation of pro-survival and inflammatory pathways is often linked to TNBC, which is defined by the lack of ER, PR, and HER2 expression. Through a variety of multi-targeted molecular pathways, curcumin predominantly inhibits PI3K/Akt/mTOR and NF-κB signaling cascades, which lowers transcription of anti-apoptotic proteins like survivin, Bcl-2, and Bcl-xL and suppresses cell growth. Additionally, it alters MAPK pathways, inhibits the epithelial–mesenchymal transition (EMT) by downregulating MMP-2, MMP-9, N-cadherin, and vimentin, and stimulates mitochondrial-dependent apoptosis through an elevated Bax/Bcl-2 ratio, cytochrome c release, and caspase-3 activation. By altering GPX4 and SLC7A11, curcumin can also increase intracellular reactive oxygen species (ROS) levels and disturb redox equilibrium, which may be a factor in ferroptosis-related signaling. Curcumin is regarded as a viable supplementary treatment candidate for the management of TNBC because of its pleiotropic mode of action, which targets the pathways for invasion, survival, proliferation, and oxidative stress all at once [8–11].

Unfortunately, curcumin's extremely poor solubility properties limit its full pharmacological potential [12]. Numerous nanostructured water-soluble delivery systems have been developed to improve the bioavailability and solubility of curcumin lately [13]. Nanotechnology can provide economic, rapid, secure, and effective ways to treat cancer and is a rapidly developing field. Nanoparticle-based platforms ensure longer blood circulation time, exceed biological barriers, and target and enhance the accumulation of drugs in tumors. Nanotechnology gives encouraging opportunities for cancer diagnosis and treatment [14, 15].

Nano drug delivery systems have the potential to overcome the obstacles of targeting a variety of cell types [16]. Graphene and graphene-based nanomaterials have become attractive in cancer treatment due to their unique chemical, physical, and mechanical properties. Furthermore, their safety and biocompatibility features enable them to be used in biological applications, including bioimaging, biosensing, diagnostics, and as anticancer drug carriers [17, 18]. In recent studies, GQDs have been employed as carriers for drug delivery in combination with electron-rich compounds via non-covalent π–π interactions [19].

In this study, newly obtained GQDs were conjugated with Cur to enhance their anticancer properties, contributing to the development of advanced therapeutic strategies. Furthermore, molecular docking analyses were performed using automated scoring functions to predict binding interactions and estimate binding affinities, while Zetasizer measurements were conducted to assess particle stability and surface charge (zeta potential) of Cur-GQDs in aqueous solution.

Experimental

Chemicals, Materials, and Instruments

Citric acid, 1,4-Bis(3-aminopropyl) piperazine, dimethylformamide (DMF), chloroform ($CHCl_3$), ethanol (EtOH), acetone, and dimethyl sulfoxide (DMSO) were purchased from Sigma-Aldrich. Deionised water (DI) was from MilliQ water. Electronic spectra were recorded on a Perkin Elmer LAMBDA 25 Series UV−vis spectrophotometer with a quartz cell of 1 cm. FTIR spectra were recorded on an attenuated total reflectance (ATR) apparatus on a Thermo Scientific Nicolet IS10-IZ10. Brookhaven Instruments 90 Plus Particle Size Analyzer was used to measure the polydispersity, particle size, mobility, and zeta potential values of GQDs and Cur-GQDs. The Smoluchowski model was selected for zeta potential measurements using an SR-542 probe. Polydispersity, particle size, mobility, and zeta potential data were obtained averages of the 10 measurements. The sample solutions were prepared by dissolving the samples in 5% (v/v) DMSO and mixing them with distilled water for pH measurements. The pH values were adjusted by the addition of various small concentrations of NaOH and HCl solutions. XRD (Panalytical X'Pert PRO) System: Source (45 kV x 40 mA)-Focusing mirror, large offset arm, detector 2θ range: 5–70 °. DTA (TA Instruments Discovery SDT 650) Analyses were performed in the range of 25–1000 °C with a heating rate of 10 °C/min in an argon gas atmosphere. Surface images were measured using a

Scanning Electron Microscope (SEM) of the JEOL JSM-7100 F model. To improve the conductivity properties of the samples, a gold-palladium (80−20%) coating process was performed in a Quorum coating device, first by applying a vacuum of 8 × 10-1 mbar/Pa and a voltage of 10 mA. Photographs were taken by applying a voltage of 15 kV. Raman spectroscopic analyses were performed using a Renishaw inVia Raman spectrophotometer (Renishaw plc, Gloucestershire, United Kingdom). The system is equipped with an Nd: YAG laser source operating at 830 nm wavelength and configured to provide 20 mW effective power, 1 µm lateral resolution, and 1–2 cm^{-1} spectral resolution. Samples were analyzed using multiple scan cumulations with a 10-second exposure time. The instrument was calibrated using a silicon (Si) reference standard, and the characteristic Raman peak (520.7 cm^{-1}) of a silicon wafer was recorded before and after each measurement to confirm the correct operation of the instrument, the accuracy of the wavenumber scale, and the stability of the laser line. This calibration procedure ensured that the error in the wavenumber scale was kept within ± 2 cm^{-1}. The spectral data obtained were graphically visualized using SpectaGraf software, and baseline correction and necessary spectral adjustments were applied to improve data quality.

Synthesis of GQDs

GQDs were synthesized using citric acid as a carbon source and 1,4-Bis(3-aminopropyl) piperazine according to the method in the literature with some modification [20]. Briefly, 1 g citric acid and 0.5 g 1,4-Bis(3-aminopropyl) piperazine were dissolved in 3 mL of DI water. The obtained solution was hydrothermally treated at 220 °C for 12 h under N_2 gas. Following the reaction, the reddish-brown mixture was filtered. This suspension was purified with a dialysis membrane (12–14 kD, Fisher Scientific) against DI water for 24 h and then precipitated in excess amount of acetone by using a centrifuge at 6000 rpm for 10 min. G-GQDs were dried in an oven at 50 °C and stored in a closed container for further applications. Finally, they were treated by a solvent-induced interface separation process using acetone. After this, the acetone solvent was evaporated, and the corresponding G-GQDs were collected after complete vacuum drying (Scheme 1).

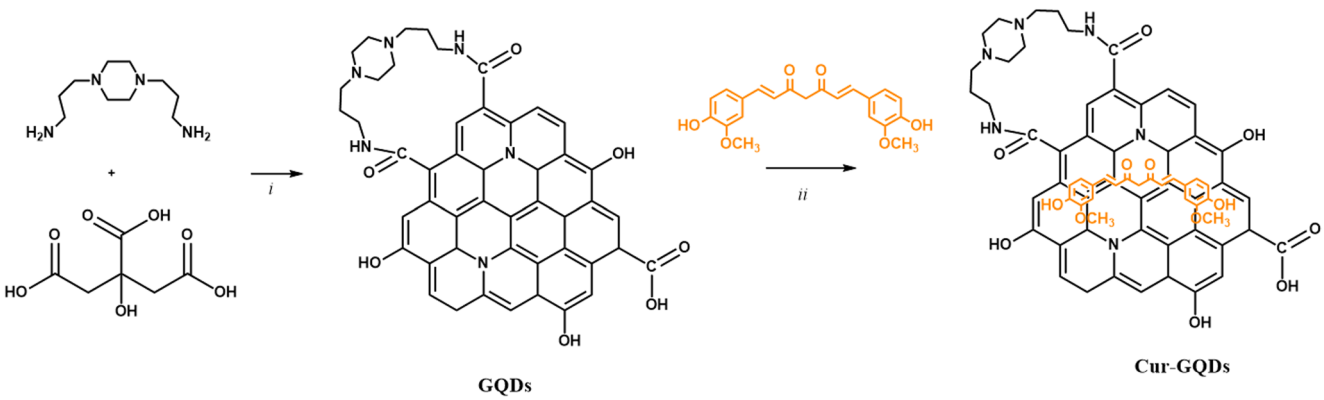
Compound Cur-GQDs Conjugate Synthesis

Curcumin conjugation of GQDs based on π-π stacking was performed by way of a slight modification to the previously reported literature [21]. Briefly, the solution of 20 mg of G-GQDs (in 1 mL H_2O) was sonicated for 1 h, and the prepared solution of 20 mg of curcumin (0.5 mL in DMF) was added into G-GQDs solution. Then, this mixture was sonicated for 4 h followed by stirring at room temperature for 4 d. The mixture was precipitated with ethanol and washed with water and ethanol. The composites were dried in a laboratory oven at 60°C to obtain Cur-GQDs (Scheme 1).

Cytotoxicity Analysis

The XTT-based cytotoxicity assay was performed using the human triple-negative breast cancer cell line MDA-MB-231 (ATCC, USA). Cells were cultured in DMEM high-glucose medium supplemented with 10% fetal bovine serum and 1% penicillin–streptomycin at 37 °C in a humidified atmosphere containing 5% CO_2.

An XTT-based cell viability assay was performed to assess the cytotoxic effects of substances on cancer cells [22]. A commercially available XTT cytotoxicity assay kit was used. XTT, in its tetrasodium salt form, is converted into a colored formazan dye by enzymes found in the mitochondria of living cells. The number of viable cells can be determined by colorimetric measurement of this colored product. In the experimental setup, 5000 cells were added



Scheme 1 Schematic illustration of conjugation of curcumin GQDs (ii) heating at 220 °C, 12 h, dialysis membrane, (i) sonicate 4 h, stir at room temperature 4 d, DMF/water

per well to 96-well plates. A cell-free control group was created by adding only medium to one column of the plate. After incubating the cells for 24–48 h, the tested substances were applied to the wells of the experimental group in serial dilutions. After application of 48 h, XTT solution containing formazan dye was added to each well, and the plates were incubated for 2 to 5 h. At the end of this period, optical density values were measured at a wavelength of 450 nm using an ELISA reader. Based on the reading data, the 50% lethal dose (LD_{50}) values of the substances on cells were calculated. Cell proliferation inhibition rates were determined using the following formula:

$$\%\ Inhibition = [(A_{450}nm\ test - A_{450}nm\ control)\ /A_{450}nm\ control] \times 100$$

Each sample was analyzed in at least three replicates.

Wound healing assay

The wound healing assay was applied to examine cell migration in vitro. This method relies on observing the ability of cells to migrate across an artificial "wound" created in monolayers of cultured cells. Wound closure rate and cell migration were assessed by microscopic imaging [23]. For this purpose, cells were incubated with 0.5% FBS-containing medium for 6 h. Then, a sterile 200 µL pipette tip was used to scratch the cell layer, and the cells were washed with PBS to remove detached cells. Following these steps, the test molecule was applied. Cell migration was monitored under an inverted phase-contrast microscope (Olympus CKX41; 50x magnification), and the closure of the wound areas over time was visualized microscopically. The data obtained were analyzed using ImageJ software (WC%) and were calculated using the following equation:

$$WC\,(\%) = [(A_o - A_t)\,/A_o] \times 100$$

where A_0 represents the initial wound area at 0 h, and A_t represents the wound area at the indicated time point. Images of the scratched areas were captured at 0, 24, and 48 h post-treatment using an inverted microscope. Cells were incubated at 37 °C in a humidified atmosphere containing 5% CO_2 during the experimental period.

Molecular Docking Analyses

Molecular docking calculations were performed in Autodock Vina software [24]. The water molecules and cofactors were removed from the protein to clearly see the protein-ligand interaction. We used VEGFA and Bcl-2 proteins, and the RCSB Protein Data Bank freely offered the structure of this protein as a 3D theoretical model (VEGFA-PDB ID: 1FLT; BCl2-PDB ID: 1GJH, https://www.rcsb.org). Protein-ligand interactions were screened by Discovery Studio 2017 Free academic (https://www.3ds.com/).

In molecular docking analysis, the selected VEGFA and Bcl-2 proteins are of particular importance due to their role in the fundamental mechanisms of cancer biology. Vascular Endothelial Growth Factor A (VEGFA) stimulates angiogenesis around tumors, meeting the oxygen and nutrient needs of cancer cells through increased expression under hypoxic conditions, thereby promoting tumor growth and metastatic potential [25, 26]. On the other hand, the Bcl-2 protein is in the mitochondrial outer membrane and suppresses the release of cytochrome c, inhibits caspase activation, stops the apoptosis process, and extends the lifespan of cancer cells [27, 28]. The common feature of these two proteins is that they increase the survival and progression capacity of tumor cells. Therefore, the selection of these proteins in molecular docking analysis holds scientific and therapeutic value for evaluating potential inhibitory compounds against both angiogenesis and apoptosis.

Results and Discussion

Synthesis and Characterization

In the first step, the GQDs were synthesized by the hydrothermal method according to the method in the literature with some modifications [20]. In the second stage, the prepared GQDs were allowed to interact with curcumin through π-π stacking reactions. The obtained nanohybrid was characterized by using various analytical techniques, including X-ray diffraction (XRD), FESEM, FT-IR, Raman, dynamic light scattering (DLS), zeta potential, and UV-vis to confirm the successful formation of the nanocomposite.

In the first step, the GQDs were synthesized by the hydrothermal method according to the method in the literature with some modifications [20]. In the second stage, the prepared GQDs were allowed to interact with curcumin through π-π stacking reactions. The obtained nanohybrid was characterized by using various analytical techniques, including X-ray diffraction (XRD), FESEM, FT-IR, Raman, dynamic light scattering (DLS), zeta potential, and UV-vis to confirm the successful formation of the nanocomposite.

FT-IR spectrum was used to confirm the transformation of the reactants into the target compounds (Fig. 1). The FTIR spectrum of GQDs reveals functional groups present at the edges/surface of graphene quantum dots. The band at 1701 cm^{-1} for GQDs is attributed to C=O vibration of the carboxyl group, while the broad bands at 3382 and 3256 cm^{-1} correspond to the presence of functional groups

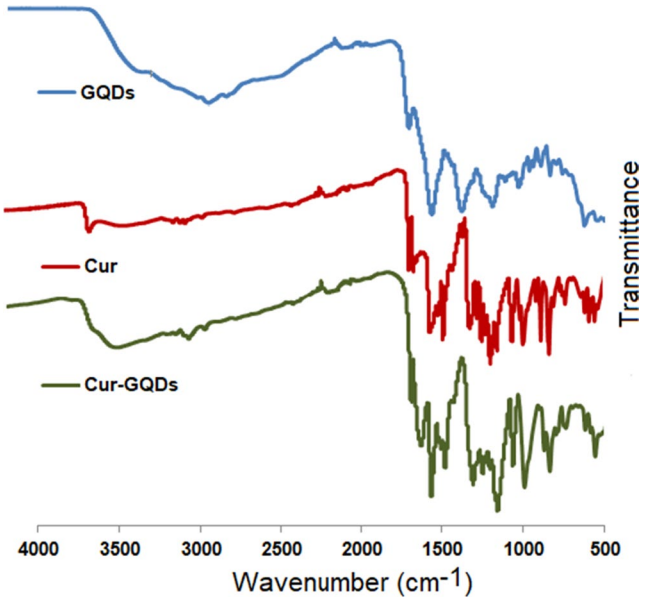


Fig. 1 FT-IR spectra of curcumin alone, GQDs alone, and Cur-GQDs

like -OH and N-H considering all the diamine structure was joined GQDs structure since there is no peak above the 1600 cm^{-1} expect for the C=O vibration of the carboxyl group, indicating there is no free NH2 group in the structure of GQDs. Peaks at 1571, 1469, 1380, 1309, 1227, and 1186, 1024 cm^{-1} can be attributed to C=C, C-C, C-N, C-O, and C-N stretching vibrations, respectively. Additionally, the peaks at 2954 cm^{-1} and 2836 cm^{-1} are associated with the asymmetric and symmetric stretching of $–CH_2$ groups. The doping of curcumin onto the GQDs was confirmed by observing the hydrogen bonding interaction between hydroxyl and carboxyl groups of GQDs and hydroxyl groups of Curcumin as well as π-π stacking between aromatic groups of GQDs and Curcumin. This is supported by the appearance of Curcumin peaks of 1625 cm^{-1}, 1600 cm^{-1}, 1505 cm^{-1}, 1272 cm^{-1} and 1024 cm^{-1} with a slight shift to 1622 cm^{-1}, 1565 cm^{-1}, 1509 cm^{-1}, 1259 cm^{-1} and 1027 cm^{-1}, respectively, confirming their successful loading of curcumin onto the GQDs.

The UV–vis absorption spectra were recorded in DMSO to characterize the GQDs, curcumin, and its conjugated forms (Fig. 2). The UV-vis absorption spectrum of GQDs shows a strong absorption peak at 260 nm, attributed to π-π* transition of the sp^2 carbon electrons in the graphene core of GQDs and another peak at 314 nm belonging to the n-π* transition of carbonyl groups [21]. The main UV-vis absorption peak of curcumin appeared at 439 nm. After hybridization of Cur with GQDs, a slight redshift in the UV-vis spectra at 444 nm, relative to the Cur alone peak, indicates the formation of composites [29].

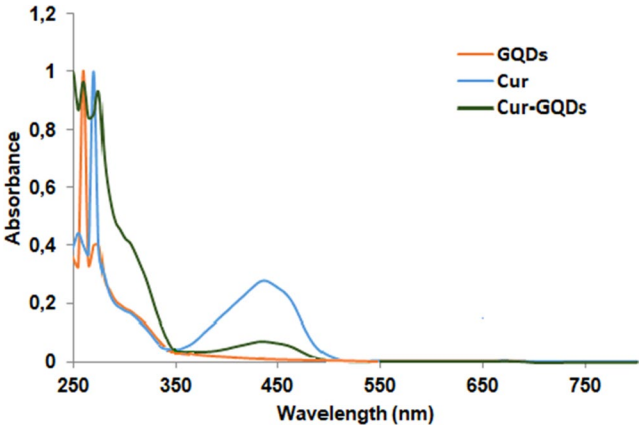


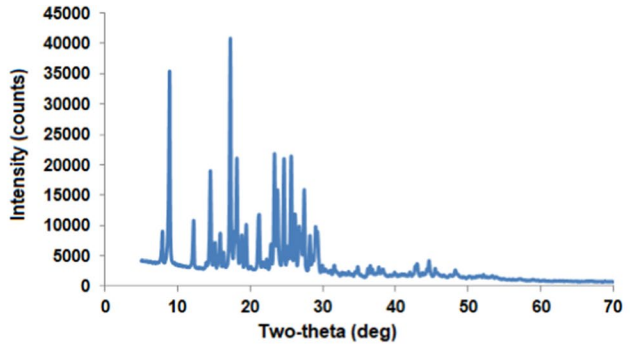
Fig. 2 Normalized electronic absorption spectra of GQDs alone, curcumin alone, and their conjugate (Cur-GQDs)

The loaded amount of the curcumin onto the GQDs was determined spectroscopically with the help of UV-Vis spectra by considering the absorption value of curcumin alone and the curcumin absorption value after loading onto the GQDs [30]. The loading of curcumin onto G-GQDs was 22%.

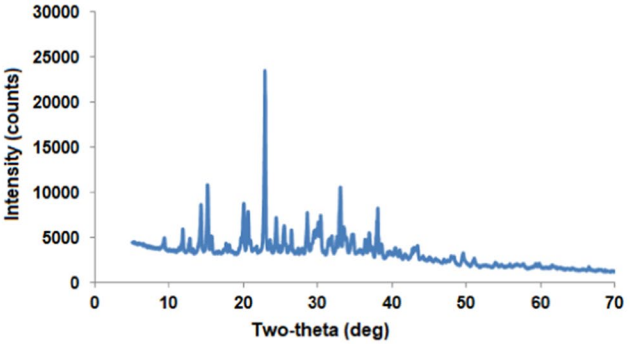
Further analysis of the GQDs and hybrid nanomaterial (Cur-GQDs) was performed using X-ray diffraction (XRD) (Fig. 3). The free curcumin demonstrated some sharp peaks at 2θ = 7.84º, 8.79 º, 12.09 º, 14.48 º, 17.19 º, 18.26 º, 23.30 º, 24.59 º, 25.69 º, 27.37 º, 28.95 º, indicating a high crystalline nature (Fig. 3a) [21]. The XRD pattern of GQDs showed the peaks near 2θ values of 14.22 º, 22.70 º, 32.91 º, 37.98 º, confirming the crystalline nature as well as hexagonal shape of GQDs. Also, the peak around 2θ = 19 ° indicates that the prepared sample is indeed a graphene quantum dot (Fig. 3b) [29]. After hybridization of GQDs with curcumin, broad diffraction peaks were observed centered at 2θ = 23.22° for Cur-GQDs. This peak could be attributed to the amorphous and disordered carbon GQDs upon conjugation [31]. The characteristic diffraction peaks of curcumin appeared at 2θ = 8.89°, 12.20°, 17.34°, 21.26°, 24.64°, 25.59°, and 29.40 °, which indicated that curcumin was still present in the Cur-GQDs in crystalline form (Fig. 3c).

Zetasizer measurements, such as particle size and zeta potential gives information about charge and stability of particles in solution [32]. To clarify the drug profile of GQDs and Cur-GQDs, Zetasizer measurements of GQDs and Cur-GQDs were performed at varying pHs. Zetasizer changes of GQDs and Cur-GQDs in water + DMSO solution with respect to pH are given in Table 1.

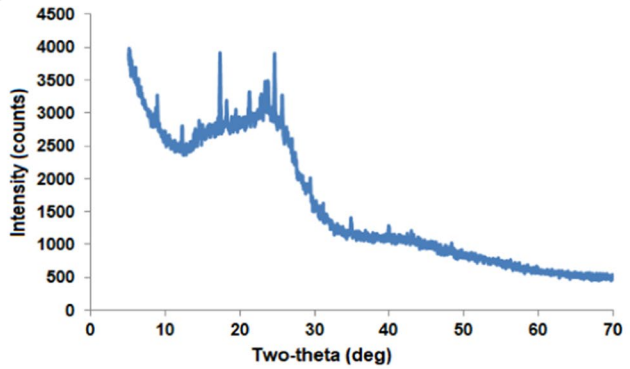
Table 1 shows that GQDs had a more uniform distribution than Cur-GQDs, with PDIs ranging from 0.04 to 0.4. The GQDs and Cur-GQDs had physical dimensions ranging



(a) Curcumin



(b) GQDs



(c) Cur-GQDs

Fig. 3 X-ray diffraction patterns of curcumin (**a**), GQDs (**b**), and Cur-GQDs (**c**). **a** Curcumin, (**b**) GQDs, (**c**) Cur-GQDs

from 10 to 15 nm, from 20 to 30 nm, with increasing pH. The GQDs and Cur-GQDs particles were negatively charged, and the zeta potentials of GQDs and Cur-GQDs were high with increasing pHs. It meant that GQDS and Cur-GQDs particles were stable in the studied pHs. The average particle sizes and zeta potentials of the GQDs and Cur-GQDs were determined to be approximately 13.7±1.7 nm and 38.4±6.2 nm, -73.62±20.6 mV and −65.5±24.3 mV, respectively, with a narrow size distribution, indicating consistent and uniform synthesis conditions. The presence of carbonyl, hydroxyl, and amino groups on the surface of

Table 1 Zetasizer changing of GQDs and Cur-GQDs in water+DMSO solution with pH

	GQDs				Cur-GQDs			
pH	PDI	Particle size (nm)	Mobility	Zeta Potential (mV)	PDI	Particle size (nm)	Mobility	Zeta Potential (mV)
2	0.46	13.4	-2.55	-33.93	0.25	21.1	-5.77	-76.67
3	0.05	12.9	-5.70	-67.33	0.31	26.1	-4.70	-60.73
4	0.05	12.1	-6.28	-70.77	0.71	33.1	-3.71	-49.32
5	0.05	10.1	-7.04	-72.92	0.21	43.8	-5.17	-68.77
6	0.05	15.3	-7.02	-93.31	0.24	24.8	-5.96	-79.19
7	0.05	15.7	-7.94	-105.53	0.22	28.6	-7.43	-98.82
8	0.28	15.1	-6.94	-92.21	0.67	32.1	-6.71	-89.16
9	0.06	13.3	-3.94	-52.41	0.55	27.8	-1.58	-20.96
10	0.05	14.6	-5.31	-71.92	0.73	24.8	-5.73	-76.14
11	0.04	14.8	-5.67	-75.33	0.34	21.6	-2.62	-34.89
Mean±SD	0.11±0.14	13.7±1.7	-6.2±1.2	73.62±20.6	0.4±0.2	38.4±6.2	-4.9±1.8	-65.5±24.3

GQD Graphene quantum dot, *PDI* polydispersity index

GQD particles in solution results in a negative charge on their surface [33].

Scanning electron microscopy (SEM) was employed to explore the morphology of the prepared products. The SEM images of curcumin powder showed irregular and needle-like crystalline particles (Fig. 4a). While the SEM image of the GQDs exhibited the agglomerated and layered structure (Fig. 4b), the SEM image of the curcumin-loaded GQDs revealed that the crystalline nature of curcumin was preserved and physically attached to the surface, which confirms the conjugation of Cur with GQDs (Fig. 4c).

The structure of curcumin, GQDs, and curcumin-loaded-GQDs (Cur-GQDs) was also investigated by Raman spectroscopy (Fig. 5). In the curcumin structure, –OH, $–OCH_3$, -C=O, and –C=C groups have important implications. The expected –C=C and –C=O vibrations were observed at 1607 cm^{-1} (aromatic -C=C) and 1629 cm^{-1} (carbonyl C=O). The peaks at 1431 cm^{-1}, 1251 cm^{-1}, and 1185 cm^{-1} belonging to the -C–O stretching of phenol, -C-O stretching of enol, and –C-O-C stretching were observed, respectively (Fig. 5a) [34]. In the Raman spectrum of GQDs (Fig. 5b), the structure is characterized by two principal bands designated as the G and D bands, which are raised at ca. 1360 cm^{-1} (D) and 1580 cm^{-1} (G), respectively, and are correlated to sp3 carbon domains and to sp2 bonds into the graphitic grid, respectively [35]. Upon conjugation of curcumin into GQDS, the observed Raman spectra revealed that the main prominent Raman bands of curcumin also appear in the spectra of Cur-GQDs with slight shifts, which confirms the conjugation except for the absence of a band specific for enol form in Cur-GQDs (Fig. 5c).

Molecular Docking Studies

According to the molecular docking analyses, significant differences were observed in the predicted binding affinities of the investigated compounds toward VEGFA and Bcl-2 proteins. Curcumin demonstrated relatively less favorable docking scores compared to the studied compounds, with calculated binding energies of −8.2 kcal/mol for VEGFA and −6.9 kcal/mol for Bcl-2; however, these values reflect in silico predictions of molecular interactions rather than direct biological potency.

However, among the new compounds examined in the study, Cur-GQDs exhibited the strongest binding affinities, with −12.4 kcal/mol to VEGFA and −11.3 kcal/mol to Bcl-2. The high binding affinity of Cur-GQDs to target proteins suggests that this compound may have a therapeutic effect on both angiogenesis inhibition and apoptosis induction, indicating that it may act as a more potent inhibitor compared to curcumin (Table 2).

A thorough examination of the docking positions showed that certain non-covalent interactions involving particular amino acid residues within the active binding pocket stabilized the ligand–receptor complexes. A hydrogen bond with Glu64 was the main mechanism of interaction in the

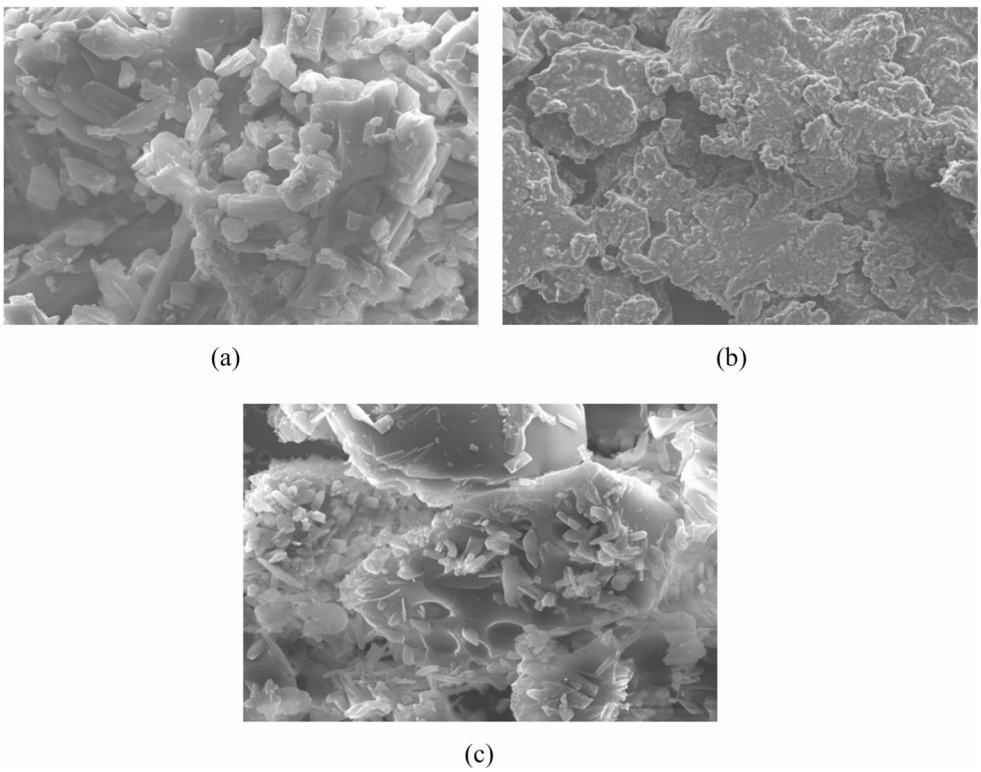
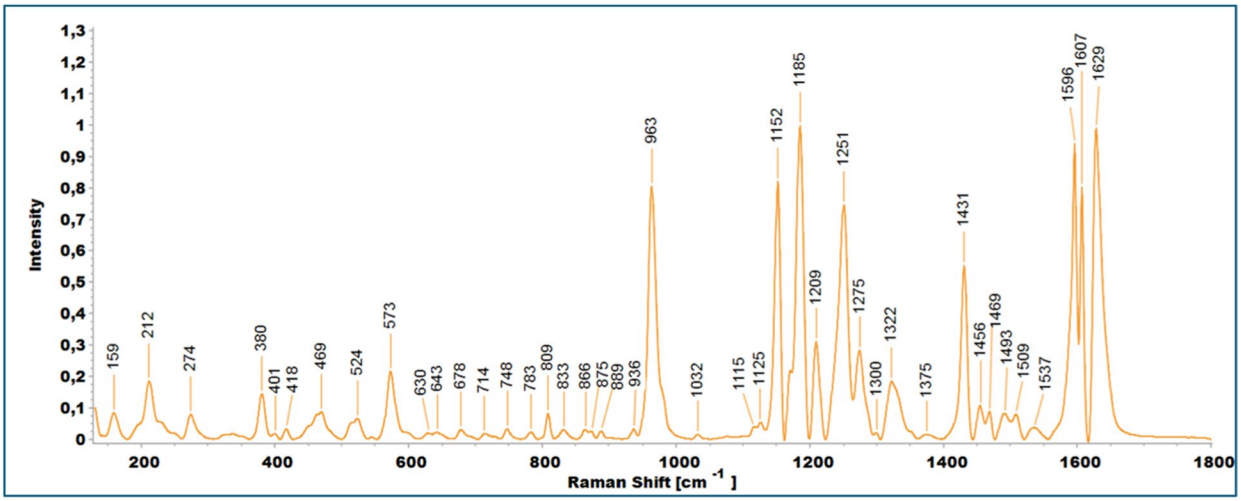
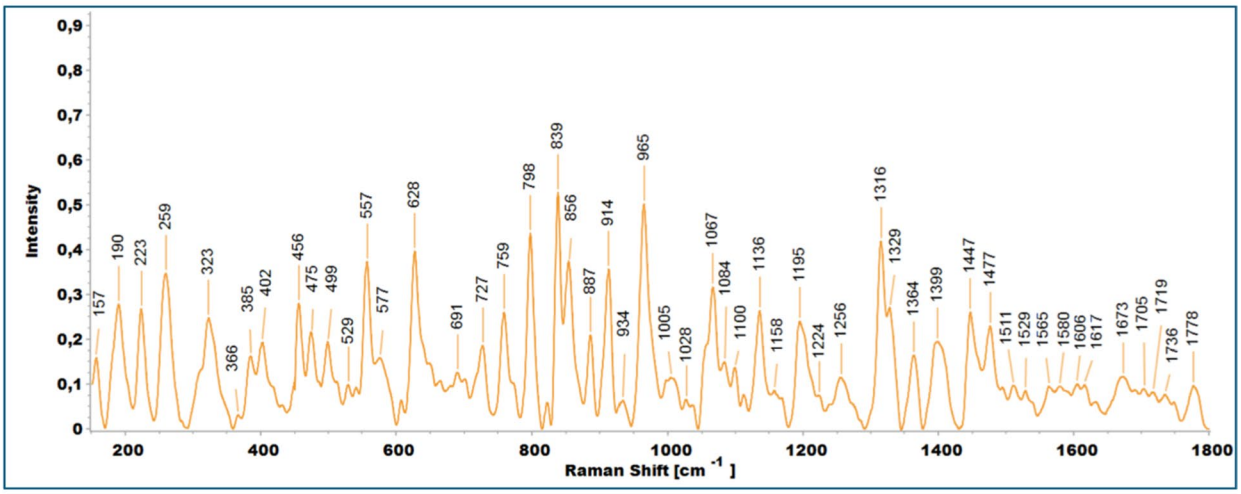


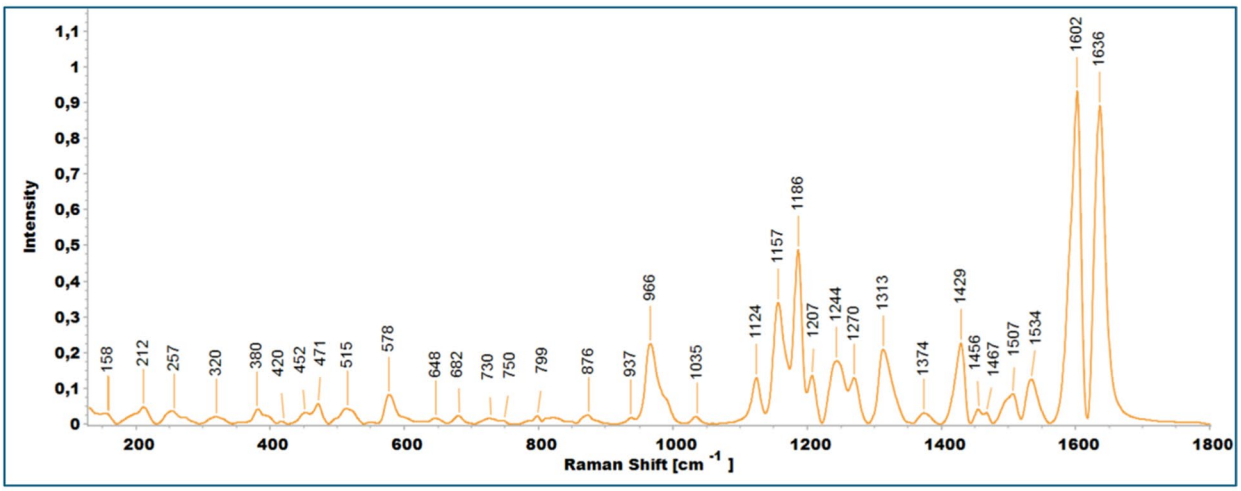
Fig. 4 Scanning electron microscopy (SEM) images of curcumin (**a**), GQDs (**b**), and Cur-GQDs (**c**)


Intensity
Raman Shift [cm -1]
159
212
274
380
401
418
469
524
573
630
643
678
714
748
783
809
833
866
875
889
936
963
1032
1115
1125
1152
1185
1209
1251
1275
1300
1322
1375
1431
1456
1469
1493
1509
1537
1596
1607
1629

(a)


Intensity
Raman Shift [cm -1]
157
190
223
259
323
366
385
402
456
475
499
529
557
577
628
691
727
759
798
839
856
887
914
934
965
1005
1028
1067
1084
1100
1136
1158
1195
1224
1256
1316
1329
1364
1399
1447
1477
1511
1529
1565
1580
1606
1617
1673
1705
1719
1736
1778

(b)

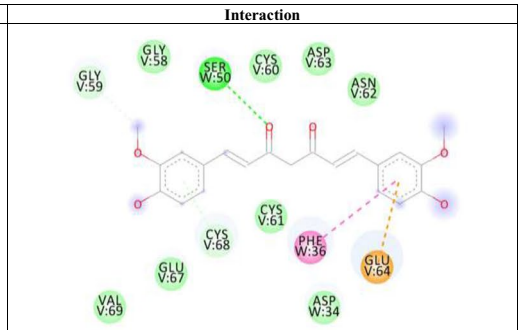
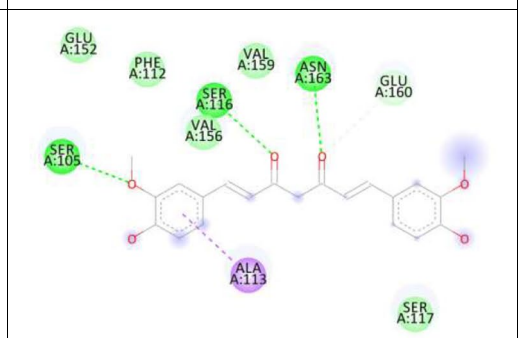
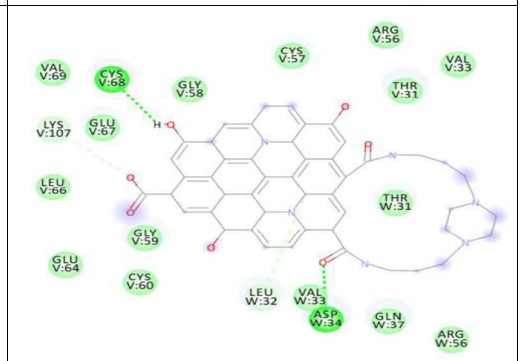
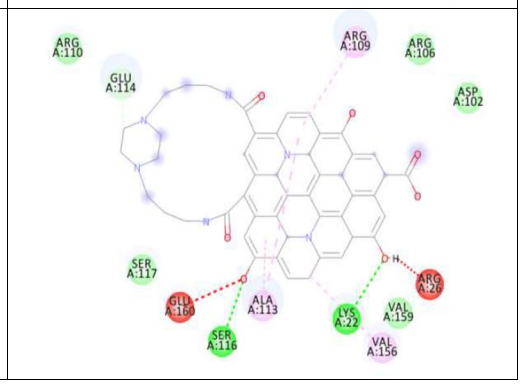

Intensity
Raman Shift [cm -1]
158
212
257
320
380
420
452
471
515
578
648
682
730
750
799
876
937
966
1035
1124
1157
1186
1207
1244
1270
1313
1374
1429
1456
1467
1507
1534
1602
1636

(c)

Fig. 5 Raman spectra of (**a**) Curcumin, (**b**) GQDs (**c**) Cur-GQDs

Curcumin–VEGFA complex. Hydrophobic interactions with Val33 and π–π stacking with Phe36 both played a role in stabilizing the binding. Three hydrogen bonds, especially with Arg105, π–π stacking interactions with Tyr67, and hydrophobic contacts with Ala146 were found in the Curcumin–Bcl-2 complex. The higher binding affinity seen in the complex may be explained by the formation of two hydrogen bonds with Lys48, as well as extra stabilization from hydrophobic interactions with Ile83 and van der Waals contacts with Leu32. The Cur-GQDs–Bcl-2 complex also showed hydrophobic contacts with Val130, π–π stacking interactions with Phe101, and two hydrogen bonds with

Table 2 Molecular docking results

Complex	Interaction
Curcumin-VEGFA	
Curcumin-Bcl2	
Cur-GQDs - VEGFA	
Cur-GQDs - Bcl2	

Asp108. Overall, the stability and binding affinity of the ligand–protein complexes were influenced by van der Waals interactions, π–π stacking, hydrogen bonding, and hydrophobic contacts.

A comparative molecular docking analysis between Cur-GQDs and therapeutically authorized small-molecule inhibitors that target the Bcl-2 anti-apoptotic and VEGF-mediated angiogenic signaling pathways was carried out to further support the therapeutic relevance of our findings. According to the investigation, Cur-GQDs engage with crucial active site residues involved in structural stabilization and functional control while occupying the typical ligand-binding sites of both proteins. Cur-GQDs were placed in VEGFA at areas linked to receptor-binding interfaces, where they formed hydrophobic and hydrogen bonding interactions with residues necessary for angiogenic activity. Like this, Cur-GQDs engaged important amino acids in Bcl-2 that are involved in anti-apoptotic protein–protein interactions through hydrophobic interactions, π–π stacking, and hydrogen bonding within the BH3-binding groove. The docking grid's XYZ coordinates were supplied to guarantee methodological reproducibility and transparency. All these results, which are corroborated by other research, support the theory that Cur-GQDs may directly modify functionally important active site domains to provide anti-angiogenic and pro-apoptotic effects (Table 3).

When the obtained findings are evaluated together with the literature, it is understood that hydrogen bonds, hydrophobic interactions, and π-based interactions play a decisive role in the interaction of curcumin and its derivatives with protein targets; that the formation of stable complexes of curcumin with target proteins by target proteins is explained especially by hydrogen bonds and π–π interactions [36] in the study by Jena et al. [36]; and that in the study by Madeswaran et al. [37], it was reported that nanoformulations containing curcumin showed higher binding affinity and biological activity thanks to various and complimentary interaction types. In this context, it is evaluated that Cur-GQDs complexes exhibit a richer interaction network consisting of strong and weak hydrogen bonds, hydrophobic and π-based interactions with lower binding energies, increasing complex stability, and yielding results consistent with the literature in terms of potential biological activity.

Statistical Analysis

The IBM SPSS Statistics 29 program was used in the study. The results obtained from two replicates were evaluated using GraphPad 8, and differences with a p-value of 0.05 were considered statistically significant.

Table 3 Detailed ligand–protein interaction profiles of curcumin and Cur-GQDs with VEGFA and Bcl2 proteins

Complex	Binding Energy (kcal/mol)	Amino Acid	Interaction Type
Curcumin–VEGFA	-8.2	SER50	Hydrogen bond
		GLU64	π–anion / electrostatic
		PHE36	π–π stacking
		CYS61	Hydrophobic
		CYS68	Hydrophobic
		VAL69	Hydrophobic
		ASP34	van der Waals
Curcumin–Bcl2	-6.9	SER105	Hydrogen bond
		SER116	Hydrogen bond
		ASN163	Hydrogen bond
		ALA113	π–alkyl
		VAL156	Hydrophobic
		VAL159	Hydrophobic
		PHE112	π–π stacking
Cur-GQDs–VEGFA	-12.4	CYS68	Hydrogen bond
		ASP34	Hydrogen bond
		THR31	Hydrogen bond
		GLY58	Weak hydrogen bond
		GLY59	Weak hydrogen bond
		VAL33	Hydrophobic
		LEU66	Hydrophobic
		VAL69	Hydrophobic
		ARG56	van der Waals
		GLU64	van der Waals
Cur-GQDs–Bcl2	-11.3	GLU160	Hydrogen bond
		SER116	Hydrogen bond
		ARG26	Hydrogen bond / electrostatic
		ARG109	π–cation
		ALA113	π–alkyl
		VAL156	π–alkyl
		LYS22	Hydrophobic

Cytotoxicity Results

According to the cytotoxicity analysis results, a statistically significant cytotoxic effect was observed in the Cur-GQDs and curcumin-treated cells compared to the control group (Fig. 6).

The 50% inhibitory concentration (IC_{50}) values of curcumin, GQDs, and Cur-GQDs were determined in the MDA-MB231 cell line. The IC_{50} values for curcumin, GQDs, and Cur-GQDs were found to be 59 µg/ml, 97 µg/ml, and 52 µg/ml in MDA-MB231 cells, respectively. These results indicate a statistically significant difference between the IC_{50} values of curcumin and Cur-GQDs compared to the control group ($P<0.05$).

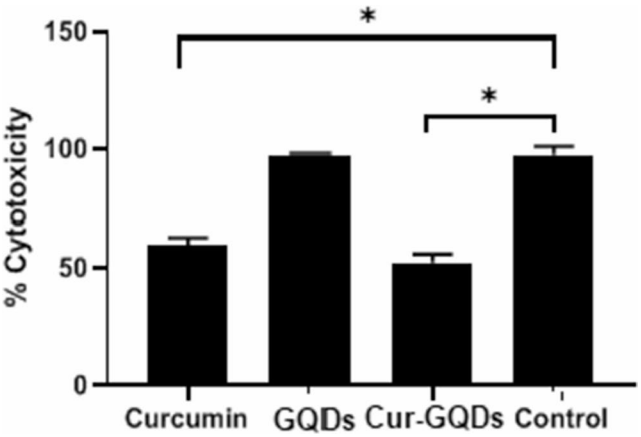


Fig. 6 Cytotoxicity analysis of Curcumin, GQDs, Cur-GQDs, *; statistically different at $p<0.05$

Migration Assay

In this study, the effects of GQD as well as Cur-GQD were examined on the migratory ability of MDA-MB-231 cells with the use of a wound-healing assay. The cell migration of MDA-MB-231 cells was observed for 24 and 48 h. According to the assay results, cell migration began in the untreated control group within 24 h (Fig. 7A), and a substantial increase in wound closure was observed by 48 h (Fig. 7B). In the control group, cells migrated efficiently.

In contrast, compared to the control group, a decrease in migration distance was observed in the cancer cells treated with GQD, Cur-GQD, and Curcumin at 24 and 48 h. The cell images observed in Figs. 8 and 9, and Fig. 10 at 24 and 48 h indicate that GQD, Cur-GQD, and Curcumin suppressed MDA-MB-231 cell migration in closing the wound gap. According to the quantitative analysis of wound closure, the most significant effect ($*p<0.05$) was observed in the Cur-GQDs combination group (Fig. 11). Migration assay exhibited that cell migration's inhibition, especially in Cur-GQD, clearly revealed impairment of cellular motility. This situation can be resembled as anti-metastatic activity. Metastasis is a fatal cause of cancer; thus, observation of decreasing migration can be a promising finding [38].

Our study used both in silico and in vitro analyses to show how Cur-GQD molecules affected cancer cells. To address curcumin's pharmacokinetic drawbacks, including its poor solubility and bioavailability, Minafra et al.

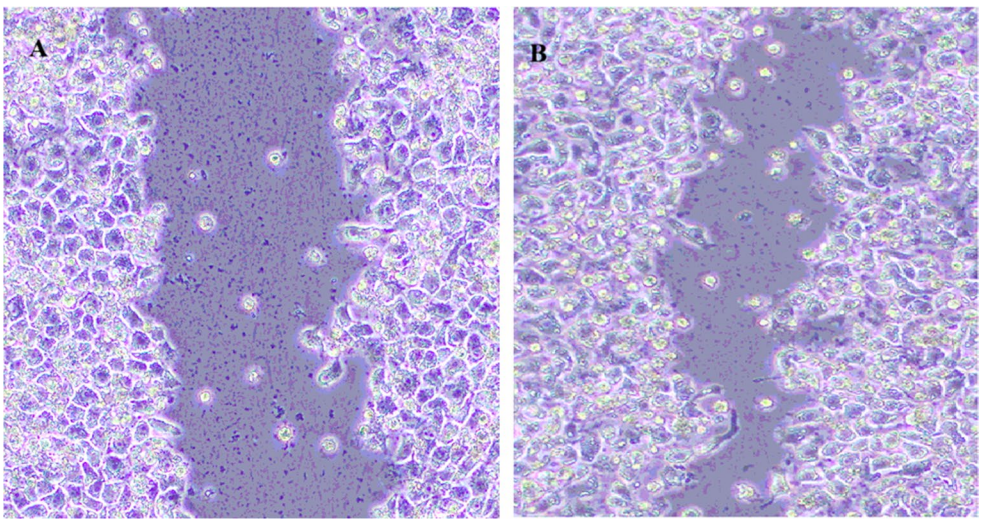


Fig. 7 Migration assay in the control group (**A**: 24 h; **B**: 48 h)

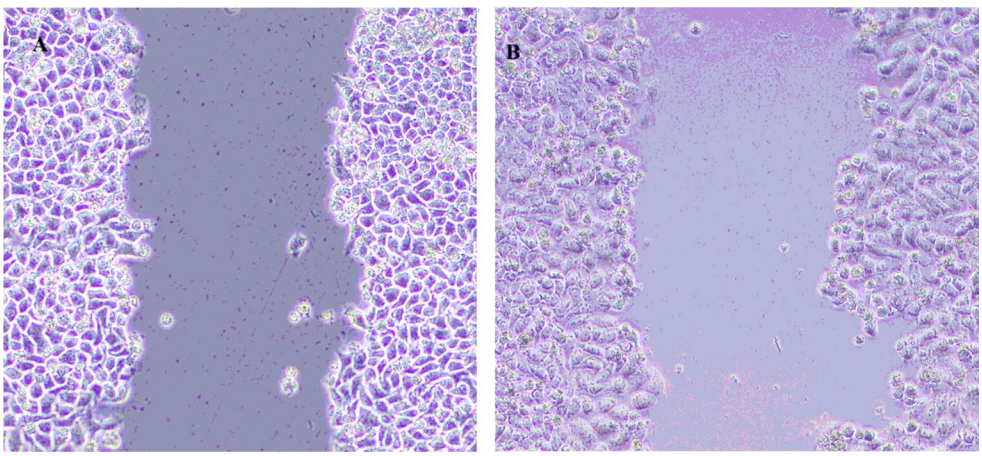


Fig. 8 Migration assay in the GQDs group (**A**: 24 h; **B**: 48 h)

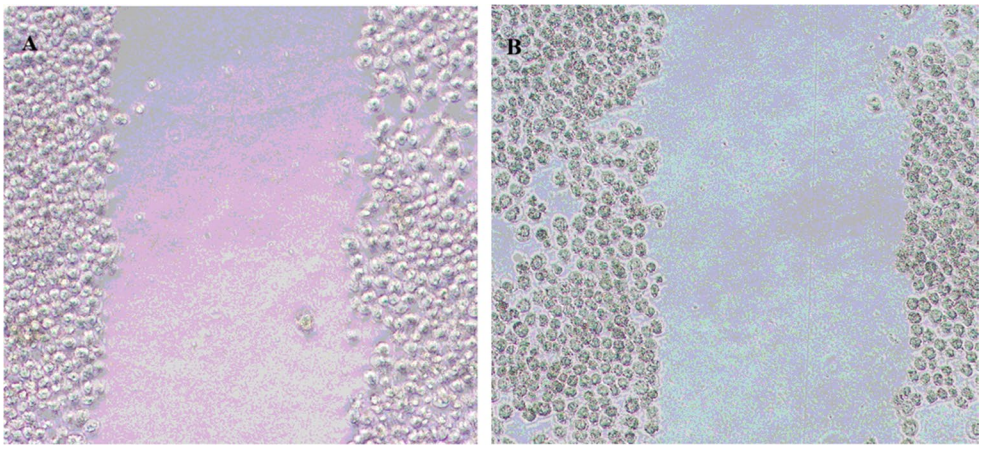


Fig. 9 Migration assay in the cur-GQDs group (**A**: 24 h; **B**: 48 h)

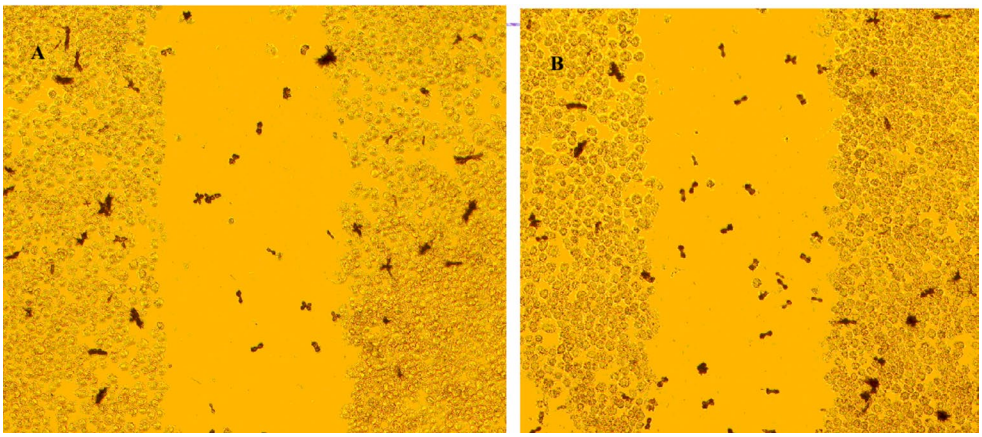


Fig. 10 Migration assay in the curcumin group (A: 24 h; B: 48 h)

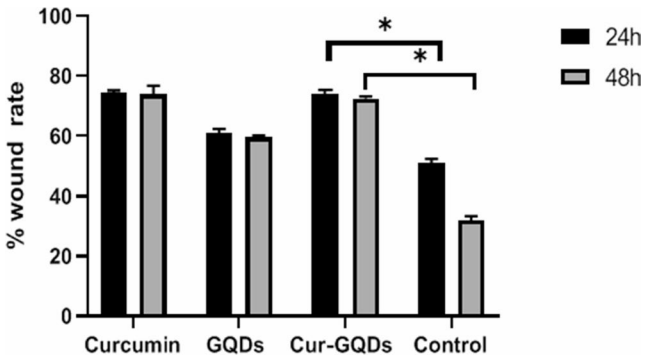


Fig. 11 Migration analysis results in cells treated with control, curcumin, GQDs, and Cur-GQDs molecules, * shows the statistical difference at $p < 0{,}05$

created curcumin-loaded solid lipid nanoparticles (Cur-SLN) and examined the formulation's therapeutic potential in conjunction with radiation therapy for breast cancer cells [39]. The MDA-MB-231 and MCF-7 cell lines were used in this investigation, and the results showed that Cur-SLNs were more efficiently absorbed by the cells and had a more potent cytotoxic effect than free curcumin. Cur-SLNs have been shown to dramatically lower cell viability, clonogenic survival, and the formation of reactive oxygen species (ROS) and DNA double-strand breaks (γH2AX), particularly when given in conjunction with radiation (2–6 Gy). Furthermore, there was a notable rise in apoptosis indicators (caspase-3 activation and PARP cleavage) and cell cycle arrest at the G2/M phase. According to researchers, these results show that the Cur-SLN formulation produces a more potent anticancer response when paired with radiation, and that lower radiation doses can still have a comparable therapeutic impact [39].

Similarly, to increase curcumin's therapeutic potential, a version of curcumin loaded into solid lipid nanoparticles was created and examined to determine how it affected breast cancer cells when paired with radiation. After characterizing the physicochemical characteristics of Cur-SLNs, they examined cytotoxicity, ROS generation, and apoptosis in breast cancer cell lines. The study's findings demonstrated that, in comparison to free curcumin, Cur-SLNs had a stronger cytotoxic effect and were more readily absorbed by cells. Together with radiation, there was a noticeable rise in the rate of apoptosis, a notable decrease in cell viability, and an increase in ROS generation. These results, according to researchers, show that the formulation of curcumin

nanoparticles acquires radio-sensitizing qualities and can be assessed as a possible adjuvant drug in the treatment of breast cancer [40].

Conclusion

According to studies, curcumin-loaded nanoparticle systems can greatly increase curcumin's therapeutic efficiency by enhancing its stability, solubility, and cellular absorption. The current study shows that conjugating curcumin with graphene quantum dots (GQDs) can increase its anticancer activity in triple-negative breast cancer cells, which is in line with these findings in the literature. Curcumin's bioavailability and interaction with target proteins were both boosted by this combination. In fact, molecular docking analyses showed that the Cur-GQDs complex had a greater binding affinity for anti-apoptotic Bcl-2, a protein essential to cell survival, and VEGFA, which is involved in tumor angiogenesis, than free curcumin. This implies that Cur-GQDs directly target the survival and proliferation pathways of cancer cells in addition to facilitating more effective intracellular transport. The particle sizes of Cur-GQDs were larger than those of GQDs, indicating that curcumin was doped monodispersely into GQDs with good particle size distribution. The relatively high negative zeta potential values (±30 mV) indicated that Cur-GQDs possessed a negative surface charge with great stability in the investigated pH range. As a result, in contrast to other curcumin-nanoparticle research in the literature, this study offers a comprehensive strategy backed by in silico molecular interaction analyses as well as cell-based cytotoxicity and migration tests. The results imply that curcumin's pharmacokinetic constraints may be addressed by nanoscale delivery systems like GQDs, opening the door to more efficient, focused, and adaptable treatment plans for aggressive triple-negative breast tumors with fewer adverse effects.

Future studies should also evaluate the safety and pharmacological potential of Cur-GQDs using ADMET prediction tools and in vitro/in vivo biocompatibility assessments to ensure safe application.

Acknowledgements We are thankful to the Department of Chemical Engineering, Uskudar University for providing necessary facilities to carry out the experiment of this work.

Author Contributions D.A. contributed to the experimental part and the writingP.S. contributed to the experimental part and writing, editing, and supervisingS.Y.A. contributed to the Cytotoxicity Analysis, writingD.Ş. contributed to some analysis and writingM.K. supervising, editing.

Funding Open access funding provided by the Scientific and Technological Research Council of Türkiye (TÜBİTAK). There is no received funding.

Data Availability No datasets were generated or analysed during the current study.

Declarations

Competing interests The authors declare no competing interests.

Open Access This article is licensed under a Creative Commons Attribution 4.0 International License, which permits use, sharing, adaptation, distribution and reproduction in any medium or format, as long as you give appropriate credit to the original author(s) and the source, provide a link to the Creative Commons licence, and indicate if changes were made. The images or other third party material in this article are included in the article's Creative Commons licence, unless indicated otherwise in a credit line to the material. If material is not included in the article's Creative Commons licence and your intended use is not permitted by statutory regulation or exceeds the permitted use, you will need to obtain permission directly from the copyright holder. To view a copy of this licence, visit http://creativecommons.org/licenses/by/4.0/.

References

1. Roy PS, Saikia BJ. Cancer and cure: A critical analysis. Indian J Cancer. 2016;53:441–2. https://doi.org/10.4103/0019-509X.200658.
2. Wang L, Li R, Song C, Chen Y, Long H, Yang L. Nat Prod Commun. 2021;16:1–42. https://doi.org/10.1177/1934578X211040326. Small-Molecule Anti-Cancer Drugs From 2016 to 2020: Synthesis and Clinical Application.
3. Xu Y, Gong M, Wang Y, Yang Y, Liu S, Zeng Q. Global trends and forecasts of breast cancer incidence and deaths. Sci Data. 2023;27:334. https://doi.org/10.1038/s41597-023-02253-5.
4. Aysola K, Desai A, Welch C, Xu J, Qin Y, Reddy V, Matthews R, Owens C, Okoli J, Beech DJ, Piyathilake CJ, Reddy SP, Rao VN. Triple negative breast cancer - an overview. Hereditary Genet. 2013;2013. https://doi.org/10.4172/2161-1041.S2-001
5. Debela DT, Muzazu SG, Heraro KD. New approaches and procedures for cancer treatment: Current perspectives. SAGE Open Med. 2021;9:1–10. https://doi.org/10.1177/20503121211034366.
6. Burguin A, Diorio C, Durocher F. Breast Cancer Treatments: Updates and New Challenges. J Personalized Med. 2021;11:808. https://doi.org/10.3390/jpm11080808.
7. Sharma RA, Gescher AJ, Steward WP. Curcumin: The story so far. Eur J Cancer. 2005;41:1955–68. https://doi.org/10.1016/j.ejca.2005.05.009.
8. Kunnumakkara AB, Bordoloi D, Harsha C. Curcumin mediates anticancer effects by modulating multiple cell signaling pathways. Clin Sci (Lond). 2017;131:1781–99. https://doi.org/10.1042/CS20160935.
9. Aggarwal BB, Sung B. Pharmacological basis for the role of curcumin in chronic diseases: an age-old spice with modern targets. Trends Pharmacol Sci. 2009;30:85–94.
10. Wahdan-Alaswad RS, Fan Z, Edgerton SM. Glucose promotes breast cancer aggression and reduces metformin efficacy. Cell Cycle. 2013;12:3759–69. https://doi.org/10.4161/cc.26641.
11. Liu Z, Ren Y, Zhang J. Role of ROS and nutritional antioxidants in human diseases. Front Physiol. 2018;9:477. https://doi.org/10.3389/fphys.2018.00477.
12. Kurien BT, Singh A, Matsumoto H, Scofield RH. Improving the solubility and pharmacological efficacy of curcumin by heat treatment. Assay Drug Dev Technol. 2007;5:567–76. https://doi.org/10.1089/adt.2007.064

13. Mohanty C, Das M, Sahoo SK Emerging role of nanocarriers to increase the solubility and bioavailability of curcumin, Expert Opin. Drug Deliv. 2012;9:1347–64. https://doi.org/10.1517/17425247.2012.724676
14. Tang X, Loc WS, Dong C, Matters GL, Butler PJ, Kester M, Meyers C, Jiang Y, Adair JH. The use of nanoparticulates to treat breast cancer. Nanomed (Lond). 2017;12:2367–88. https://doi.org/10.2217/nnm-2017-0202.
15. Dessale M, Mengistu G, Mengist HM. Nanotechnology: A Promising Approach for Cancer Diagnosis, Therapeutics and Theragnosis. Int J Nanomed. 2022;26:3735–49. https://doi.org/10.2147/IJN.S378074.
16. Rajesh S, James LW. Nanoparticle-based targeted drug delivery. Exp Mol Pathol. 2009;86:215–23. https://doi.org/10.1016/j.yexmp.2008.12.004
17. Zuchowska A, Chudy M, Dybko A, Brzozka Z. Graphene as a new material in anticancer therapy-in vitro studies. Sens Actuators B. 2017;243:152–65. https://doi.org/10.1016/j.snb.2016.11.105.
18. Tian P, Tang L, Teng KS, Lau SP. Graphene quantum dots from chemistry to applications. Mater Today Chem. 2018;10:221–58. https://doi.org/10.1016/j.mtchem.2018.09.007.
19. Zhang XF, Shao X. π–π binding ability of different carbon nanomaterials with aromatic phthalocyanine molecules: Comparison between graphene, graphene oxide and carbon nanotubes. J Photochem Photobio A: Chem. 2014;278:69–74. https://doi.org/10.1016/j.jphotochem.2014.01.001.
20. Liu J, Zhang X, Cong Z, Chen Z, Yang H, Chen G. Glutathione-functionalized graphenequantum dots as selective fluorescent probes for phosphate-containing metabolites. Nanoscale. 2013;5:1810–5. https://doi.org/10.1039/C3NR33794D.
21. De D, Das CK, Mandal D, Mandal M, Pawar N, Chandra A, Gupta AN. Curcumin Complexed with Graphene Derivative for Breast Cancer Therapy, ACS Appl. Bio Mater. 2020;3:6284–96. https://doi.org/10.1021/acsabm.0c00771.
22. Jörg W, Lochmann D, Zimmer A. A practical note on the use of cytotoxicity assays. Int J Pharm. 2005;288:369–76. https://doi.org/10.1016/j.ijpharm.2004.09.018.
23. Justus CR, Leffler N, Ruiz-Echevarria M, Yang LV. In vitro cell migration and invasion assays. J visualized experiments. 2014;88:51046. https://doi.org/10.3791/51046.
24. Trott O, Olson AJ. AutoDock Vina: improving the speed and accuracy of docking with a new scoring function, efficient optimization, and multithreading. J Comput Chem. 2010;31:455–61. https://doi.org/10.1002/jcc.21334.
25. Ferrara N. Vascular endothelial growth factor. Arterioscler Thromb Vasc Biol. 2009;29:789–91. https://doi.org/10.1161/ATVBAHA.108.179663.
26. Apte RS, Chen DS, Ferrara N. VEGF in signaling and disease: beyond discovery and development. Cell. 2019;176:1248–64. https://doi.org/10.1016/j.cell.2019.01.021.
27. Cory S, Adams JM. The Bcl2 family: regulators of the cellular life-or-death switch. Nat Rev Cancer. 2002;2:647–56.
28. Delbridge ARD, Strasser A. The BCL-2 protein family, BH3-mimetics and cancer therapy. Cell Death Differ. 2015;22:1071–80. https://doi.org/10.1038/cdd.2015.50.
29. Bansal S, Singh J, Kumari U, Kaur IP, Barnwal RP, Kumar R, Singh S, Singh G, Chatterjee M. Development of biosurfactant-based graphene quantum dot conjugate as a novel and fluorescent theranostic tool for cancer. Int J Nanomed. 2019;14:14809–818. https://doi.org/10.2147/IJN.S188552.
30. Shih-Chen S, Hsin-Hung L, Tao-Hsing C, Chih-Kuang C, Bao-Tsan K. Preparation of aldehyde-graphene quantum dots from glucose for controlled release of anticancer drug. Front Mater. 2023;10:1–8. https://doi.org/10.3389/fmats.2023.1180745.
31. Safardoust-Hojaghana H, Amirib O, Hassanpoura M, Panahi-Kalamueia M, Moayedic H, Salavati-Niasar M. Food Chem. 2019;295:530–5. https://doi.org/10.1016/j.foodchem.2019.05.169.
32. N, Joudeh D, Linke. Nanoparticle classification, physicochemical properties, characterization, and applications: a comprehensive review for biologists. J Nanobiotechnol. 2022;20:262. https://doi.org/10.1186/s12951-022-01477-8.
33. Madhi A, Hadavand BS. Fluorescent epoxy-graphene quantum dots nanocomposites: synthesis and study of properties. Polymer-Plastics Technol Mater. 2022;61:117–30. https://doi.org/10.1080/25740881.2021.1959929
34. Singh AK, Prakash P, Singh R, Nandy N, Firdaus Z, Bansal M, Singh RK, Srivastava A, Roy JK, Mishra B. Singh, Curcumin Quantum Dots Mediated Degradation of Bacterial Biofilms Front. Microbiol. 2017;8:1517. https://doi.org/10.3389/fmicb.2017.01517.
35. Rivera LM, Fajardo S, Arévalo MC, García G, Pastor E. S- and N-Doped Graphene Nanomaterials for the Oxygen Reduction Reaction. Catalysts. 2017;7:278. https://doi.org/10.3390/catal7090278.
36. Jena AB, Kanungo N, Nayak V, Chainy GBN, Dandapat J. Catechin and curcumin interact with S protein of SARS-CoV-2 and ACE2 of human cell membrane: Insights from computational studies. Sci Rep. 2021;11:2043. https://doi.org/10.1038/s41598-021-81462-7
37. Madeswaran A, Tamilazhagan S, Mohan S. In silico evaluation, characterization, and in vitro anticancer activity of curcumin–nimbin loaded nanoformulation in HCT-116 cell lines. BioTechnologia. 2024;105(4):355–65. https://doi.org/10.5114/bta.2024.145256.
38. Stuelten CH, Parent CA, Montell DJ. Cell motility in cancer invasion and metastasis: insights from simple model organisms. Nat Rev Cancer. 2018;18:296–312. https://doi.org/10.1038/nrc.2018.15.
39. Minafra L, Porcino N, Bravatà V, Gaglio D, Cammarata FP, Forte GI, Pisciotta P, Manti L. Radiosensitizing effect of curcumin-loaded lipid nanoparticles in breast cancer cells. Sci Rep. 2019;9:11134. https://doi.org/10.1038/s41598-019-47553-2.
40. Sak K. Radiosensitizing Potential of Curcumin in Different Cancer Models. Nutr Cancer. 2020;72:1276–89. https://doi.org/10.1080/01635581.2019.1681480.

Publisher's Note Springer Nature remains neutral with regard to jurisdictional claims in published maps and institutional affiliations.